Aalto University

OPEN ACCESS

This is an electronic reprint of the original article.
This reprint may differ from the original in pagination and typographic detail.

Trogen, Mikaela; Le, Nguyen Duc; Sawada, Daisuke; Guizani, Chamseddine; Lourençon, Tainise Vergara; Pitkänen, Leena; Sixta, Herbert; Shah, Riddhi; O'Neill, Hugh; Balakshin, Mikhail; Byrne, Nolene; Hummel, Michael

Cellulose-lignin composite fibres as precursors for carbon fibres. Part 1 – Manufacturing and properties of precursor fibres

Published in:
Carbohydrate Polymers

DOI:
10.1016/j.carbpol.2020.117133

Published: 15/01/2021

Document Version
Peer-reviewed accepted author manuscript, also known as Final accepted manuscript or Post-print

Published under the following license:
CC BY-NC-ND

Please cite the original version:
Trogen, M., Le, N. D., Sawada, D., Guizani, C., Lourençon, T. V., Pitkänen, L., Sixta, H., Shah, R., O'Neill, H., Balakshin, M., Byrne, N., & Hummel, M. (2021). Cellulose-lignin composite fibres as precursors for carbon fibres. Part 1 – Manufacturing and properties of precursor fibres. *Carbohydrate Polymers*, *252*, Article 117133. https://doi.org/10.1016/j.carbpol.2020.117133

This material is protected by copyright and other intellectual property rights, and duplication or sale of all or part of any of the repository collections is not permitted, except that material may be duplicated by you for your research use or educational purposes in electronic or print form. You must obtain permission for any other use. Electronic or print copies may not be offered, whether for sale or otherwise to anyone who is not an authorised user.

Journal Pre-proof

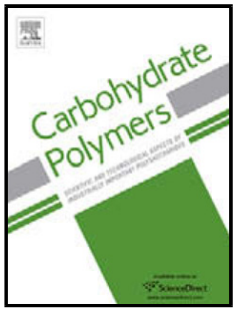

Cellulose-lignin composite fibres as precursors for carbon fibres. Part 1 – Manufacturing and properties of precursor fibres

Mikaela Trogen (Conceptualization) (Investigation) (Formal analysis) (Visualization) (Writing - original draft), Nguyen-Duc Le (Resources) (Writing - review and editing), Daisuke Sawada (Investigation) (Formal analysis) (Visualization) (Writing - review and editing), Chamseddine Guizani (Formal analysis) (Writing - review and editing), Tainise Vergara Lourençon (Investigation) (Formal analysis) (Writing - review and editing), Leena Pitkänen (Investigation) (Formal analysis) (Writing - review and editing), Herbert Sixta (Resources) (Supervision), Riddhi Shah (Investigation) (Writing - review and editing), Hugh O'Neill (Resources) (Writing - review and editing), Mikhail Balakshin (Resources) (Writing - review and editing), Nolene Byrne (Resources) (Supervision) (Writing - review and editing), Michael Hummel (Supervision) (Funding acquisition) (Conceptualization) (Resources) (Writing - review and editing)

PII: S0144-8617(20)31306-0

DOI: https://doi.org/10.1016/j.carbpol.2020.117133

Reference: CARP 117133

To appear in: *Carbohydrate Polymers*

Received Date: 4 July 2020

Revised Date: 14 September 2020

Accepted Date: 18 September 2020

Please cite this article as: Trogen M, Le N-Duc, Sawada D, Guizani C, Lourençon TV, Pitkänen L, Sixta H, Shah R, O'Neill H, Balakshin M, Byrne N, Hummel M, Cellulose-lignin composite fibres as precursors for carbon fibres. Part 1 – Manufacturing and properties of precursor fibres, *Carbohydrate Polymers* (2020), doi: https://doi.org/10.1016/j.carbpol.2020.117133

This is a PDF file of an article that has undergone enhancements after acceptance, such as the addition of a cover page and metadata, and formatting for readability, but it is not yet the definitive version of record. This version will undergo additional copyediting, typesetting and review before it is published in its final form, but we are providing this version to give early visibility of the article. Please note that, during the production process, errors may be discovered which could affect the content, and all legal disclaimers that apply to the journal pertain.

© 2020 Published by Elsevier.

Journal Pre-proof

Cellulose-lignin composite fibres as precursors for carbon fibres. Part 1 – Manufacturing and properties of precursor fibres

Mikaela Trogen[a], Nguyen-Duc Le[b], Daisuke Sawada[a], Chamseddine Guizani[a], Tainise Vergara Lourençon[a], Leena Pitkänen[a], Herbert Sixta[a], Riddhi Shah[c], Hugh O'Neill[c], Mikhail Balakshin[a], Nolene Byrne[b] and Michael Hummel[a]

a) Aalto University, School of Chemical Engineering, Department of Bioproducts and Biosystems, P.O. Box 16300, 00076 Aalto, Finland
b) Institute for Frontier Materials, Deakin University, Geelong, Vic 3217, Australia
c) Neutron Scattering Division, Oak Ridge National Laboratory, Oak Ridge, TN 37831, USA

ABSTRACT

Cellulose-lignin composite fibres were spun from ionic liquid (IL) solutions by dry-jet wet spinning. Birch pre-hydrolysed Kraft (PHK) pulp and organosolv beech (BL) or spruce lignin (SL) were dissolved in the IL 1,5-diazabicyclo[4.3.0]non-5-enium acetate ([DBNH]OAc) to prepare spinning dopes. Fibres with lignin concentrations of up to 50% were spun successfully. The fibres were analysed focusing on important properties for the production of carbon fibres (CF). Due to the higher molar mass of the SL compared to the BL, SL showed higher stability in the spinning process, giving higher lignin content in the final fibres. The CF yield after carbonization increased with increasing lignin content. The higher carbon content of SL compared to BL, resulted in moderately higher CF yield of the SL fibres, compared to fibres with BL. Overall, the produced cellulose-lignin composite fibres show great potential as precursors for CF production.

Keywords
Ionic liquid Spinning Fibres Precursor Carbon fibres

Journal Pre-proof

Journal Pre-proof

1. Introduction

In recent years, many political decisions have been made and ambitious goals set to reduce the use of fossil raw materials and to lower the carbon dioxide emissions. To achieve these goals, we need to produce lighter, more fuel-efficient vehicles, using raw materials and fuels from renewable sources. Carbon fibres (CFs) show desirable weight-to-strength ratio and are applicable for production of lightweight composite materials to substitute heavier metal parts in vehicles. Therefore, there is a growing market which is dominated by CFs made from polyacrylonitrile (PAN) precursor fibres (PFs) since the 1970s. These fibres have many benefits, for instance excellent strength, and high chemical and temperature resistance. The major drawbacks of PAN CFs are the high price, as well as the use of fossil raw materials and toxic chemicals in the manufacturing process (Frank, Steudle, Ingildeev, Spörl, & Buchmeiser, 2014). In the production of PAN CFs, the cost of the precursor makes up approximately 50 % of the total cost of the CF (Baker & Rials, 2013). Today, there is also a growing market for lightweight materials, for instance, in the automotive and sports industries, where top-end strength properties are less significant than a competitive price. Therefore, CFs made from wood PFs have become highly interesting. The first cellulose PFs in use consisted of vegetable fibres, such as cotton thread and were utilised as the filament in electric lamps (Edison, 1880; Swan, 1880). Cellulose PFs drew much attention from the 1950s to the 1970s, but the research activity declined after the discovery of PAN-derived CFs (Frank et al., 2014). With the consumption and environmental pressure rising equally fast, lignocellulosic precursors deserve to be revisited for CF production.

Cellulose as PF comes with a few challenges, one being the low carbon yield. In theory, every anhydroglucose unit (AGU) can release five molecules of water during the dehydration process. This corresponds to a mass yield loss of 55.6% and gives a theoretical carbon yield of only 44.4%. However, during the carbonization process cellulose undergoes several different degradation reactions, resulting in loss of CO_2, CO and other low-molar-mass carbon compounds.

Journal Pre-proof

Consequently, the carbon mass losses may add up to 90 % of the original carbon content (Frank et al., 2014). Nevertheless, cellulose being a renewable material with an established production of regenerated cellulose fibres for the textile industry (Sayyed, Deshmukh, & Pinjari, 2019) is still an interesting candidate as a PF for CF production. The properties, the structure and orientation, of the polymers in the PFs directly affect the structure and properties of the CFs (Edie, 1998; Frank et al., 2014; Goldhalm, 2012). In previous years, mainly wet-spun cellulosic viscose fibres were utilised as precursors. Standard viscose fibres show some significant shortcomings for CF production, such as an irregular cross section, a low degree of polymerisation (DP) and low orientation in the fibres, which limit the mechanical properties of the resulting CFs (Röder et al., 2009). Nevertheless, in the early phase of CF development highly oriented viscose fibres could be converted to CFs with tensile strengths of 1 – 4 GPa and moduli of 170 – 690 GPa when graphitized at 2500 °C (Thornel series) (Morgan, 2005; Prosen, 1970). Commercial Lyocell fibres are produced by dissolving wood pulp in *N*-methylmorpholine *N*-oxide monohydrate (NMMO) and the dope is spun using a dry-jet wet spinning process. Lyocell fibres, with a circular cross section and high polymer orientation depict significantly better fibre strength properties than standard viscose fibres (Röder, Moosbauer, Wöss, Schlader, & Kraft, 2013).

Next to cellulose, lignin is the second most abundant polymer in plants and the lignin content in wood typically ranges from 20 to 30 %. While cellulose exhibits a well-defined structure of linear polymer chains, enabling high orientation of the polymers in the PFs, lignin consists of a complex and variable molecular network, hindering polymer orientation within the PFs. The lack of orientation results in PFs with lower strength properties as compared to pure cellulose PFs. The lignin polymer is built up by p-coumaryl, coniferyl and sinapyl alcohol precursors and its structure depends on the wood species and its position in the tree trunk (Baillères, Castan, Monties, Pollet, & Lapierre, 1997; Balakshin, Capanema, & Chang, 2008; Fagerstedt et al., 2015; Koch, 2006). In addition, the structure of industrial lignin also varies with the process conditions used to isolate it

Journal Pre-proof

(Berlin & Balakshin, 2014). Lignin possesses a significantly higher carbon content (60-65%) (Ház et al., 2019; Hosseinaei, Harper, Bozell, & Rials, 2016) than cellulose. Therefore, CFs with lignin can give higher carbon yields. Lignin fibres can be produced with different spinning methods, for instance, melt (Foston et al., 2013; Norberg, Nordström, Drougge, Gellerstedt, & Sjöholm, 2013), dry (M. Zhang & Ogale, 2014) and dry-jet wet spinning (Bengtsson et al., 2018). Lignin can serve as a precursor for CF production and can be used as single raw material or blended with other polymers, such as PAN (B. Zhang et al., 2019), nanocellulose (Wang et al., 2019), cellulose (Bengtsson et al., 2018; Ma et al., 2015) as well as a mixture of cellulose and hemicellulose (Nypelö, Asaadi, Kneidinger, Sixta, & Konnerth, 2018).

Softwood lignins (SWL) consist mainly of guaiacyl building blocks, while hardwood lignins (HWL) feature a blend of guaiacyl and syringyl moieties (Koch, 2006). Due to this difference in composition, HWL contains higher amounts of β-O-4 linkages, giving it a more linear structure compared to SWL (Brodin, Sjöholm, & Gellerstedt, 2009). The guaiacyl building blocks in SWL feature a high amount of 5-5'-biphenyl units and β -5 moieties, leading to a more condensed and cross-linked structure (Balakshin et al., 2020; Kadla et al., 2002; Kubo & Kadla, 2005b). For these reasons, HWL has successfully been melt spun, while the condensed structure of SWL impairs melt spinning (Kadla et al., 2002). Kadla *et al.* attempted melt spinning of softwood kraft lignin (SW-KL) but found that SW-KL charred instead of melting during heating from 140 to 240°C (Kadla et al., 2002). Also, Kubo and Kadla reported problems in melt spinning of SW-KL. It failed to melt, but transformed into a rubbery material at temperatures above 250°C. This rubbery material with very high viscosity was unsuitable for melt spinning (Kubo & Kadla, 2005a). Some of the issues of lignin melt spinning can be resolved by using synthetic or organic softening agents. Kubo and Kadla successfully melt spun SW-KL by mixing it with poly(ethylene oxide) (PEO). To achieve continuous fibre spinning with high take-up speeds, more than 50% of PEO was required (Kubo & Kadla, 2005a). Nordström *et al*. used hardwood kraft lignin permeate (HKLP) as softening agent in melt

Journal Pre-proof

spinning SW-KL. By adding 3–95% HKLP to SW-KL continuous filaments could be spun successfully (Nordström, Norberg, Sjöholm, & Drougge, 2013). Melt-spun lignin fibres also require long stabilisation times before carbonization. Mainka *et al.* reported stabilisation times of several days, in laboratory conditions, for melt-spun HWL fibres. In semi-production scale and by tuning of the thermal profile, they manage to reduce the stabilisation time from ~150 h to ~100 h. However, in order to achieve acceptable process economics, the stabilisation time needs to be reduced to only a few hours (Mainka et al., 2015).

In dry-jet wet spinning, the polymers are dissolved in a solvent, such as NMMO or an ionic liquid (IL). The polymer solution is spun through an air-gap into a regeneration bath, forming Lyocell-type fibres. Therefore, by using the dry-jet wet spinning technique, difficulties in melting the lignin can be bypassed. It allows the use of both SWL (Bengtsson et al., 2018) and HWL (Ma et al., 2015) In the last few years, several articles have been published on the Ioncell® process (Hummel et al., 2016; Sixta et al., 2015). In this process the biopolymers are dissolved in the IL (1,5-diazabicyclo[4.3.0]non-5-ene acetate, [DBNH]OAc) and the fibres are dry-jet wet spun. [DBNH]OAc can dissolve a wide range of biopolymers, including essentially all wood biopolymers. Ma *et al.* (Ma et al., 2015; Ma et al., 2016) and Nypelö *et al.* (Nypelö et al., 2018) showed that, in addition to cellulose also lignin- and hemicellulose-containing Ioncell® fibres can be spun. Although the application focus of these fibres has been set on textile fibres (Haslinger, Hummel, Anghelescu-Hakala, Määttänen, & Sixta, 2019; Ma et al., 2016) Byrne *et al.* showed that Ioncell® fibres are also suitable for the production of carbon fibres (Byrne, De Silva, Ma, Sixta, & Hummel, 2018; Byrne et al., 2016). The group of Sjöholm has shown that cellulose-lignin PFs are suitable for carbon fibre production and studied various stabilisation and carbonization protocols (Bengtsson et al., 2018; Bengtsson, Bengtsson, Sedin, & Sjöholm, 2019; Bengtsson et al., 2020). Herein, we present results of a systematic study on using Ioncell® cellulose-lignin PFs, focusing on decisive structural properties of the precursor filaments for the production of CFs. The carbon yield could be

Journal Pre-proof

improved substantially through even distribution of lignin in the cellulose matrix. No spin finish or carbonization aid was used to fully elucidate the interplay and synergistic effects of the wood polymers. Organosolv lignins, free from sulphur and prehydrolysed kraft pulp (dissolving pulp) with low hemicellulose and lignin content were used as well defined raw materials. Detailed investigations on the carbon fibre production are then reported in part 2 of this study.

2. Experimental

2.1 Materials

Pre-hydrolysed kraft (PHK) birch pulp ([η] = 494 ml/g) was received from Stora Enso Enocell mill in Finland and Organosolv (ethanol/H_2SO_4) beech lignin (BL) and spruce lignin (SL) from the Lignocellulosic Biorefinery Pilot Plant, Fraunhofer CBP in Leuna, Germany. The pulp was received as sheets and ground using a Wiley mill to a fine powder. The lignin was used as received. For the preparation of IL, 1,5-diazabicyclo[4.3.0]non-5-ene (DBN) (Fluorochem, UK) and acetic acid (glacial, 100%, Merck, Germany) were used. DBN and acetic acid were used as received. Tap water, cooled to 9±2°C, was used in the spin bath.

2.2 Spinning process

The preparation of IL and dope as well as fibre spinning were performed with the Ioncell® process according to previously published methods, with only few modifications (Hummel et al., 2016; Ma et al., 2015). The IL 1,5-diazabicyclo[4.3.0]non-5-enium acetate ([DBNH]OAc) was always prepared on the same day as the spin dope. DBN was mixed with acetic acid in a 2-liter glass reactor with cooling (25°C) and after the slow addition of acid the solution was mixed for an hour at 75°C. Pulp and lignin were dissolved in the IL using a vertical kneader (80°C, 90 min, 7±3 mbar, mixing 30 rpm). The dissolved cellulose or cellulose-lignin mixtures (dopes) were filtered (pore size 5 µm) using a filter press. The filtered dope was dry-jet wet spun using a piston-spinning unit (Fourné Polymertechnik, Germany), with an air gap of 1 cm. A spinneret with 400 holes, capillary diameter 100 µm and L/D 0.02 was used. The extrusion rate in the spinning process was 5.5 ml/min and the

Journal Pre-proof

temperature 71±5°C. PFs with different cellulose-lignin ratios and different draw ratios (DR) were spun (Table 1). Higher total polymer concentrations were needed for the solutions containing 30 - 50% of lignin to maintain suitable rheological properties and ensure stable spinning conditions (Ma et al., 2015). After spinning, the fibres were washed with tap water using a custom-made washing line (washing: 10±0.25 min retention time at 68±3°C; drying: 80°C).

2.3 Carbonization of precursor fibres

Carbonization laboratory tests were performed using a NBD-O1200 (NBD Tech, USA) oven with nitrogen gas atmosphere. The temperature was raised from 20°C to 900°C at a rate of 10°C/min. The temperature was held at 900°C for 60 min before the tube chamber was allowed to cool to room temperature. The PFs were carbonized without any pre-treatment and no tension was applied on the fibres during carbonization.

2.4 Carbohydrate and lignin analysis

The sample preparation for carbohydrate and lignin analyses were performed according to the NREL/TP-510-42618 standard and the samples were analysed using an ion chromatograph (ICS-3000 HPAEC-PAD) with a Dionex™ CarboPac™ PA20 column (ThermoFisher Scientific, USA). The eluent used was water and after each analysis, the column was washed with NaOH, followed by water for regeneration of the analysis conditions before the next injection. The acid-soluble lignin (ASL) was determined by using a Shimadzu UV 2550 spectrophotometer at 205 nm. The results for the pulp and the spun fibres were calculated according to procedures published by Janson (Janson, 1970). The results for the lignin samples were calculated as the total amount of carbohydrates and total amount of lignin as per cent on dry sample.

2.5 Molar mass distribution

The molar mass distribution of carbohydrates was determined using a Dionex Ultimate 3000 HPLC module, with a Shodex differential refractive index (DRI) detector (model RI-101) and a

Journal Pre-proof

Viscotek/Malvern SEC/MALS 20 multi-angle light-scattering (MALS) detector. The columns used were Agilent PLgel MIXED-A (x 4). As eluent, 0.9% LiCl in DMAc was used with a flow rate of 0.75 ml/min. The samples were prepared using a solvent exchange procedure (water/acetone/DMAc) and finally dissolved in eluent (0.9% LiCl/DMAc). The injection volume was 100 µl and sample concentration around 1 mg/ml. The detector constants (MALS and DRI) were determined using a narrow polystyrene sample (M_w = 96 000 g/mol, Đ = 1.04) dissolved in 0.9% LiCl in DMAc. A broad polystyrene sample (M_w = 248 000 g/mol, Đ = 1.73) was used for checking the detector calibration. The ∂n/∂c value of 0.136 ml/g was used for celluloses in 0.9% LiCl in DMAc (Potthast et al., 2015). For the determination of molar mass distribution of lignin, an Agilent 1100 HPLC system, equipped with an UV detector (280 nm) was used. The columns used were Polymer Standards Service MCX 300 X 8 mm (three columns with pore sizes of 100Å, 500Å, 1000Å). The eluent used was 0.1 M NaOH with a flow rate of 0.7 ml/min. The injection volume was 50 µl. The calibration curve was accomplished with polystyrene sulfonate standards (1000 – 64000 g/mol) and syringol (M = 154 g/mol).

2.6 Mechanical properties

The mechanical properties of the PFs were measured using a Favigraph single-fibre tester (Textechno H. Stein GmbH & Co. KG, Germany) according to the standard SFS-EN 5079 with only minor modifications. The PFs were conditioned in 20±2°C and 65±2 % RH overnight prior to the mechanical testing. The following conditions were used for the testing: Load cell 20 cN, gauge length 20 mm and test speed 20 mm/min. For each sample, 20 fibres were measured.

2.7 Birefringence

The birefringence was measured using a Zeiss Axio Scope A1 polarised light microscope with a Leica B 5λ-Berek tilting compensator. For the measurement, three filaments were taped on a microscope slide with two pieces of double-sided tape. The optical retardation was determined in duplicate from three selected spots on each filament. The linear density was measured using a TexTechno

Journal Pre-proof

Favigraph single fibre tester. Also, for the linear density, three filaments were measured three times. The diameter was calculated assuming a density of 1.5 g/mL (Lenz, Schurz, & Wrentschur, 1994) for cellulose and 1.4 g/mL for lignin (Ehrnrooth, 1984; Stamm, 1929). Birefringence Δn is defined as the retardation divided by the diameter. The total orientation was calculated by dividing Δn by 0.062, which is the maximum birefringence of cellulose (Lenz et al., 1994). For cellulose-lignin blends, the measured results from the carbohydrate-lignin analysis (Table 3) were used to adjust the birefringence to the actual cellulose content.

2.8 Small-angle x-ray scattering (SAXS)

Synchrotron X-ray scattering data were collected at beamline D2AM at European Synchrotron Radiation Facility (ESRF, Grenoble, France). The fibre samples were mounted on a tailor-made multi-position fibre sample holder. Small angle X-ray scattering patterns (SAXS) were collected in the transmission mode using flat 2D detector "XPAD-D5" (imXPAD, France). The X-ray energy was set to 18 keV (λ = 0.688801 Å). The sample to detector distance was calibrated using silver behenate. Data were processed using pyFAI (Ashiotis et al., 2015), a python library for azimuthal integration of diffraction data. Data were corrected for the detector distortion, the incident beam intensity and the scattering contribution from air.

Equatorial intensity profiles of SAXS data were obtained from the azimuthal integration. The range of integration was determined by fitting equatorial streaks at the scattering vector Q = 0.01 $Å^{-1}$ using a pseudo-Voigt function. The fitted profile was used to estimate the disorientation parameter of small angle X-ray scattering (f_{saxs}) using the same conversion protocol as WAXD data processing. Then, the double range of the full width half maximum was set for the range of integration. The equatorial intensity profiles were fitted by a power law function, or a combination of power law function and Guinier scattering for the scattering vector Q-range of 0.007 - 0.18 $Å^{-1}$ using a unified fit function (Beaucage, 1995) implemented in SasView software (Doucet et al., 2017):

Journal Pre-proof

$$I(Q) = \sum_{i=1}^{N} \left[G_i \exp\left(-\frac{Q^2 {R_{gi}}^2}{3} \right) + \exp\left(-\frac{Q^2 {R_{g(i+1)}}^2}{3} \right) B_i \left(\frac{1}{{Q_i}^*} \right)^{P_i} \right] + background \quad (1)$$

$${Q_i}^* = Q \left[\mathrm{erf}\left(\frac{Q R_{gi}}{\sqrt{6}} \right) \right]^{-3} \quad (2)$$

where G_i and B_i are the scaling parameter, R_{gi} is the radius of gyration and P_i is the exponent of the power law part. Meridional intensity profiles were prepared from narrow range to avoid the equatorial scattering contribution, which was 10° by azimuthal angle from the centre of meridional scattering. The meridional intensity was fitted with a power law function.

2.9 SEM

A Zeiss Sigma VP instrument was used for the SEM imaging. To obtain an image of the cross section the fibres were prepared by cryofracture. A bundle of fibres was first taped across a shallow aluminium cup and the cup was filled with water. The cup was dipped into liquid nitrogen until the water froze, leaving the fibre bundles inside the ice cube. The ice cube was removed from the container and then cracked in the middle. The fractured fibre bundles were allowed to thaw and dry before attaching them onto the conductive support with carbon tape. The samples were sputter-coated with gold to ensure electric conductivity. The images were taken at 3kV operating voltage.

2.10 Thermogravimetric analysis

Thermogravimetric analysis (TGA) was made using a Netzsch STA 449 F3 Jupiter & QMS 403 Aëolos Quadro thermal analyser with helium atmosphere. The temperature program was set from 40°C to 800°C, with a heating rate of 10°C/min. A Matlab script was created for data treatment. The following parameters were extracted: T_{onset} (the temperature at the weight loss of 5%), T_{peak} (the temperature at the maximum mass-loss rate). DTG_{peak} (the maximum mass-loss rate) and T_{offset} (the temperature at a weight loss of 95%).

2.11 Elemental analysis

Journal Pre-proof

The elemental analysis was performed using a Perkin Elmer Series II 2400 CHNS/O analyser. Carbon (C), nitrogen (N) and hydrogen (H) content of all PFs and of some selected CFs were determined.

More details on the experimental procedures for NMR and WAXD are described in the Supporting Information, Section 1.

3. Results and discussion

3.1 Raw materials

Composition and molar mass of the pulp and lignin samples can be found in Table 2. SL shows higher molar mass and slightly higher lignin content than BL.

NMR spectroscopy indicated that SL and BL were rather similar to previously described OH group analysis by ^{31}P NMR spectroscopy (Figure S1 and Table S1, in SI, Section 2) and showed very similar amount of aliphatic OH, total phenolic OH and carboxyl groups. The lignin species differed foremost in the type of phenolic OH. As expected, BL showed a higher content of 5-substituted phenolic-OH groups (sum of S- and condensed G-phenolic units), attributed to the syringyl moieties. The analyses of the lignins via HSQC 2D NMR showed (Figure S2, in SI) that qualitatively the structures of the organosolv BL and SL were very similar to that reported earlier (Balakshin et al., 2010a, 2010b, 2010c; Berlin et al., 2006). Therefore, the quantification of ^{13}C NMR spectra was performed by the same algorithm (Balakshin & Capanema, 2015).

Comprehensive analysis of different lignin functionalities by quantitative ^{13}C NMR analysis (Table S2 and Figure S3, in SI) showed, as expected, a higher content of methoxy groups in BL due to the contribution of the S-units. The degree of condensation was significantly higher for SL, i.e. typical for SWLs when compared to HWLs. The amounts of oxygenated aliphatic moieties was about 1.5 times higher in BL. The amounts of other functionalities were rather similar in SL and BL. Surprisingly, the lignins studied have very similar quantities of different functional groups examined with a comprehensive NMR approach except the presence of S-units in the HW lignin.

Journal Pre-proof

Therefore, all differences in their properties and performance can be predominantly attributed to more branched/crosslinked nature of the SW lignin and its higher potential to be crosslinked further (e.g., during stabilization/carbonization) via the 5-position in the aromatic ring.

3.2 Properties of PFs

The chemical composition of the raw materials and PFs was determined in order to follow the changes in composition during the spinning process. The Enocell pulp, the main component of the PFs comprises 91.7% cellulose, 7.7% hemicelluloses and 0.6% lignin. The BL and SL consist of 96.4% (BL) / 97.1% (SL) lignin and 0.3% (BL) / 0.5% (SL) carbohydrates. The compositions of the precursors are shown in Table 3. The theoretical lignin values in Table 3 were calculated using the lignin content of the raw materials shown in Table 2. The lignin content of the PFs are slightly different from the calculated theoretical values. During the spinning process, some water-soluble parts of lignin were lost (Table 3). These lignin fractions either did not coagulate in the spin bath or were leached out during the washing process. The lignin loss is approximately double in E90-SL10 compared to E70-SL30. If the same ratio is expected to happen for BL, E90-BL10 should have a lignin loss of approximately 15.5%. However, BL having a lower average molar mass than SL got more readily lost during the spinning process. Lignin deprivation is also connected to the thickness of the filaments. At constant draw, the fibres differed in their titer due to the inevitable variation of the total polymer concentration in the spin dope. This might to some extent also explain the extraordinarily high relative loss in the E90-BL10 sample.

Figure 1 shows the tenacities of the PFs at different draw ratios. Cellulose and its macro-structural organization in the fibres has the biggest effect on the mechanical properties. In a dry-jet wet spinning process, the liquid filaments are typically stretched in the air gap before they enter the coagulation bath. This so-called draw exerts uniaxial stress on the polymer solution, which causes the cellulose to adopt a preferential alignment parallel to the filament axis. Increasing draw leads

to higher cellulose orientation. The lignin moieties are considerably smaller than the cellulose chains. They virtually dilute the cellulose matrix and counteract the effects of cellulose orientation. Consequently, pure cellulose fibres had the highest tenacity and the tenacity decreases with increasing lignin content. The type of lignin has no significant influence on the tenacity. The tenacity follows the cellulose content of the fibre. Only a slight increase in tenacity can be seen between DR 3 and DR 12. The major change in orientation of the fibres takes place below DR 3. Therefore, also the strength properties of the fibres develop below DR 3 and start to level off upon further increase of draw. This behaviour was also found by Nypelö *et al.* (Nypelö et al., 2018). The crystallographic parameters for E100 PFs are shown in Table S3 (SI, Section 3). All samples in the DR range of 3-12 showed similar crystallographic parameters, which explains the similar tenacities of these fibres. Hence, most filaments were spun at moderate DR to minimize the occurrence of filament breaks in the air gap (Hummel et al., 2016; Ma et al., 2016).

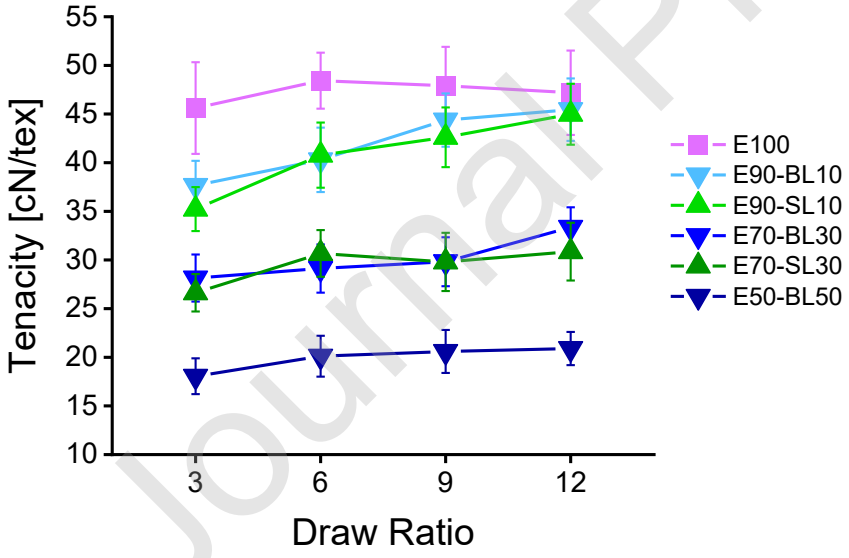

Figure 1. Effect of draw ratio DR on the tenacity (tensile strength) of PFs with different lignin content.

Figures S4a and S4b (SI, Section 4) present the elongation of the PFs at different draw ratios. The elongation increases with the addition of lignin. For BL (Figure S4a), this relationship is more

Journal Pre-proof

evident than for SL (Figure S4b). Ma *et al.* also found that an increase in lignin content leads to lower tenacity and higher elongation (Ma et al., 2015; Ma et al., 2016). Both tenacity decrease and elongation increase upon rising lignin content in the fibre can be attributed to a "dilution" of the cellulose matrix with lignin. Being considerably smaller than the average cellulose chains, lignin does not contribute notably to the mechanical properties of the composite fibres (Hummel et al., 2018). At DR 12, fibres with BL (70:30, DR 12) showed a tenacity of 33.4 ± 2.1 cN/tex and the fibres with SL (70:30, DR 12) a tenacity of 30.9 ± 3.0 cN/tex. These values correspond well to the values published by Ma *et al.* They reported a tenacity value of 30.1 ± 3.6 cN/tex (at DR 12.6) for a fibre containing eucalyptus PHK pulp and organosolv BL (70:30) (Ma et al., 2015).

The crystallographic parameters of PFs (DR3) with different concentration of lignin are listed in Table 4. Through correlation of the anisotropic and isotropic scattering of the sample, it was possible to quantify the cellulose content in the fibre, herein termed cellulose content index CEL.I. The cellulose fibre (E100) showed a value lower than 100, probably due to the presence of small amounts of isotropic cellulose and hemicellulose fractions. The CEL.I. values generally agreed with the measured cellulose content of PFs shown in Table 3, confirming the increased retention of SL in the composite fibres as compared to BL.

The obtained C.I.EQ. values were much higher than C.I. values found in previous reports because of the different calculation, taking only a selected range of the azimuthal scan into account (indicated by the extension EQ). For details see SI, which also includes the crystallinity indices calculated via the classical azimuthal integration over the entire 360° range (Table S4). The scale of C.I. and C.I.EQ. values are different but showed the desired relative consistency throughout all samples.

Journal Pre-proof

Figure 2 depicts the total and weighted orientation of the PFs with varying lignin content. A steady decrease in orientation with increasing lignin content was observed until reaching a value of 0.304 ± 0.016 (E50-BL50, DR 6) for fibres with 50% beech lignin. This is in good agreement with Ma *et al*., who reported a value of 0.304 (at DR 5.3) for a fibre containing eucalyptus PHK pulp and organosolv beech lignin (50:50) (Ma et al., 2015). The total fibre orientation is calculated from the birefringence of polarized light passing through the fibre. The wavelength retardation depends on the orientation of the cellulose matrix in the fibre and on the fibre thickness. The birefringence is then obtained by dividing the retardation by the fibre thickness and the total orientation by further division with the maximum birefringence of cellulose, 0.062. However, lignin is not an optically anisotropic materials and as such not birefractive. The decline of the measured orientation upon gradual addition of lignin can thus be due to the reduction of optically anisotropic material in the light path and due to reduced orientation of the cellulose matrix. Therefore, the orientation values were divided by the measured cellulose fraction in the respective fibre (Table 3). These weight-normalised values did not change much up to 30% for both lignin types, indicating that the actual cellulose part in the fibres has the same total orientation. The WAXD results discussed below were in line with these observation. Upon 50% lignin content, however, the total orientation dropped below a value that could be only attributed to the reduced amount of birefractive material. The cellulose matrix in the E50-BL50 composite fibre had a notably reduced orientation.

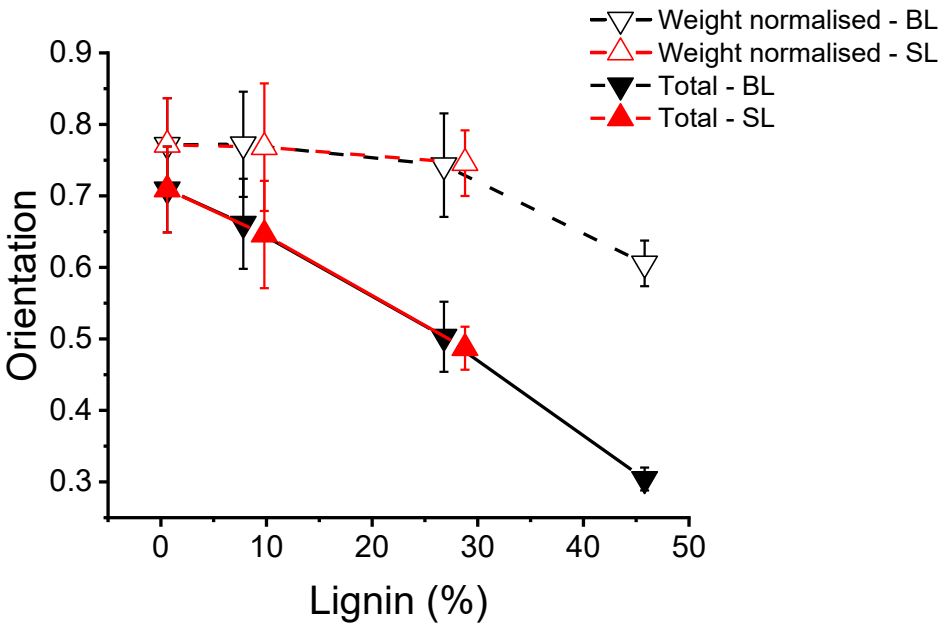

Figure 2. Total and weight-normalised orientation of PFs (DR 6) with different lignin content.

WAXD analyses were conducted to elucidate the structural characteristics of the PFs. The crystallinity index (C.I.EQ.) and Hermans orientation parameter as well as average crystal width of three equatorial planes ($(1\bar{1}0)$, (110) and (020)) are given in Table S3 (SI, Section 3). The C.I.EQ. values were extracted from the azimuthal integration of the equatorial section of the fibre diffraction pattern. The resulting C.I.EQ. values are notably higher than C.I. values reported earlier (Asaadi et al., 2018; Sixta et al., 2015) and crystallinities estimated by azimuthal averaging over the 360 degree range (Table S4, in SI, Section 3). Thus, the C.I.EQ. values cannot be used to quantify the volume fraction of crystalline domains in the material, but the relative consistency among the highly oriented samples can be assured. A merit of using a fibre diffraction pattern instead of the powder diffraction method is the preliminary subtraction of lignin scattering. In this approach, we could access the change of cellulose crystallinity without (or minimal) contribution of lignin scattering.

In line with the weighted orientation, Hermans parameters for the orientation of crystalline cellulose decreased only moderately up to a lignin concentration of ca. 30%, but dropped notably

Journal Pre-proof

for the fibre with 50% BL. It is possible that a high amount of heterogeneous lignin molecules can alter the response of a cellulose solution to extensional stress. The local stress tensor acting on the cellulose molecules could be reduced, resulting in a lower orientation of the linear polymer chains in the filament before coagulation in the spin bath. However, the crystal widths (Ave. CW) of cellulose crystallites were similar for all PFs. Reduced orientation during the spinning process itself should also affect the shape of crystal. Therefore, it is more likely that a high concentration of lignin impairs the alignment of cellulose fibrils due to associations between lignin molecules and cellulose fibrils during the coagulation process. This is also supported by the SEM images of the cross section (Figure 3). In the cross section of the E100 samples, the typical fibrillar structure can be clearly seen, while in the E50-BL50 the fibre body shows a more ductile appearance.

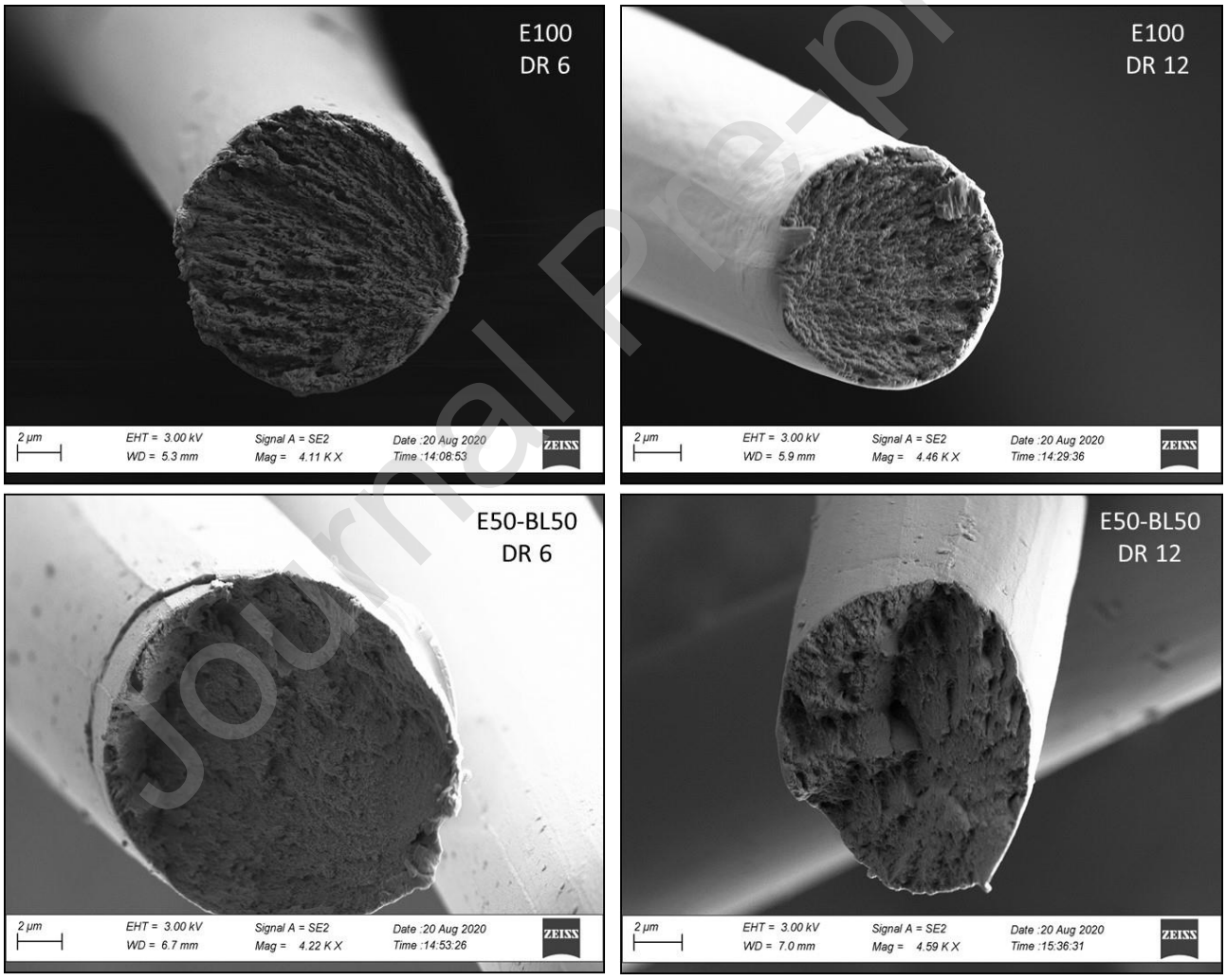

Figure 3. SEM images of cross sections of precursor fibres.

Journal Pre-proof

In the coagulation process, the lignin molecules did not interfere with the horizontal crystallite growth of cellulose II reflected by the nearly constant crystallite size for all lignin types and concentrations. Contrary, the crystallinity index followed the trend of the change of orientation by the concentration of lignin. This index intends to express the volume fraction of crystalline cellulose over the total cellulose because the scattering contribution of lignin has already been removed beforehand in the data reduction process. The amount of amorphous cellulose is almost constant up to a lignin concentration of 30% while the significant increase of amorphous cellulose was plausible for 50% BL sample.

The structure of the lignin-cellulose composite fibres was further examined by small angle X-ray scattering. The X-ray scattering pattern showed anisotropy due to the fibrillar assembly of the cellulose matrix. Figure S5 (SI, Section 5) shows the 2D small angle X-ray scattering pattern of cellulose and lignin-cellulose composite fibres. Because of the anisotropy, the intensity profiles were analysed in equatorial and meridional directions (Figure S6 and Table S5, in SI). The equatorial streak of dry fibre samples has been attributed to the surface scattering generated by microvoids (Sharma, Sen, Thakre, & Kumaraswamy, 2019; Vickers, Briggs, Ibbett, Payne, & Smith, 2001). For E100, the equatorial scattering intensity was indeed represented by a power law decay with an exponent of 3.9. This power law function with an exponent close to 4 can be attributed to the scattering of the smooth surface of microvoids. The meridional section of the fibres showed a similar power law decay with an exponent ranging from 2.0 to 2.6 with high fitting error. The changes of exponent with the addition of lignin were difficult to explain. We do not have a conclusive interpretation of the meridian scattering for the moment.

For equatorial scattering of the composite fibres, an additional increase of the scattering intensity at scattering vectors $Q > 0.2$ Å^{-1} was observed beyond the line of the power law function. This was anisotropic scattering because it was not observed in the meridian direction. Taking into account

Journal Pre-proof

the presence of lignin, particle or aggregates of lignin molecules in cellulose fibrils likely cause the additional scattering contrast and increased the scattering intensity at this Q-range.

The different particle sizes of the lignin types were a prominent feature of these samples. The radius of gyration of E70-BL30 and E70-SL30 in equatorial direction was estimated to be 75 and 56 Å with small standard errors, respectively. These scattering features were not observed in the narrow meridian area, indicating that this scattering feature was anisotropic. Langan et al. demonstrated that lignin molecules in poplar form globular aggregates (150 – 200 Å in radius) after steam explosion pre-treatment (Langan et al., 2014), and that the scattering resulting from these aggregates was isotropic. It is likely that the anisotropic scattering of lignin aggregates is a result of the spinning process creating a highly oriented cellulose matrix. The length information of the aggregates could not be obtained in this study because such structural information was overlapped with the strong central scattering due to the contrast between microvoids and the cellulose matrix. Further studies with contrast control will be needed to unravel the structure of at least three-phase composite materials.

Lignin molecules have been found in cylindrical shape, for example, in dimethyl sulfoxide (DMSO), DMSO with polyethylene glycol (Imel, Naskar, & Dadmun, 2016), and in ethylene glycol solvents (Yang, Zhao, Singh, Simmons, & Cheng, 2019). The vertical alignment of lignin aggregates might be accelerated by such cylindrical subunits, but the cylindrical radius of ca. 7 Å was out of the Q-range in this study and it would likely overlap with the scattering from the cellulose elementary fibrils in lignin-cellulose composite fibres.

3.3 Carbonization

The behaviour of the PFs during carbonization and the final CF yield play a crucial role for CF production. Lignin features a significantly higher carbon content than cellulose, leading to higher carbon content of the PFs with increasing lignin amount (Figure 4a). SL exhibits a moderately higher relative amount of carbon than BL. Consequently, PFs containing SL also show slightly

Journal Pre-proof

higher carbonization yield than fibres with BL (Figure 4b). The purpose of this study was to investigate the behaviour of the different raw materials during carbonization and therefore no finishing agents or additives were used. The CF yields could be further increased by applying some pre-treatment like common flame retardants on the fibres before the pyrolysis (Bengtsson et al., 2019; Bengtsson et al., 2020; Unterweger, Hinterreiter, Stifter, & Fuerst, 2018).

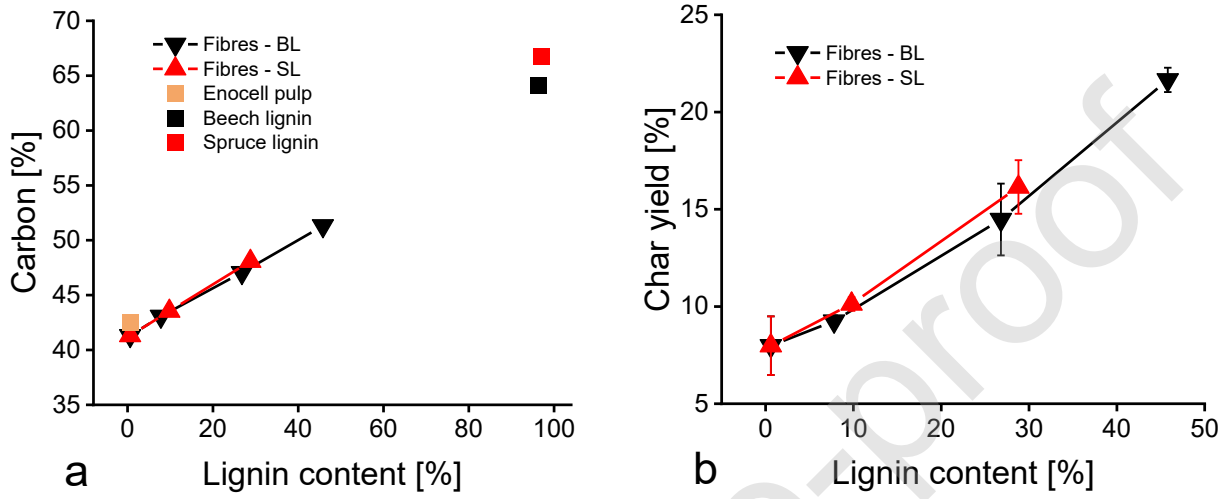

Figure 4. (a) Carbon content of PFs and raw materials (CHN elemental analysis) and (b) yield after carbonization (in oven). No pre-treatments were performed before carbonization and no tension was applied on the fibres during carbonization.

The TGA results (Figure 5) also fall in line with the other findings. The final weight-% increases with higher lignin content in the PFs and SL gives higher char yields than BL (Figure 5a).

The NMR results explain the higher char yield in the case of SL and SL containing fibres compared to the BL and its respective composite fibres. At temperatures higher than 200 °C, lignin pyrolysis and devolatilization is a melt phase radical process, in which reactivity is ruled principally by the competition between initiation, propagation and termination reactions of different propagating radicals. The NMR results show that SL is mainly composed of guaiacyl units, which are more prone to radical condensation/recombination reactions during pyrolysis in comparison to the hardwood BL, which have substantially higher amount of syringyl units bearing additional

Journal Pre-proof

methoxyl groups that limit the extent of the radical recombination reactions and hence lower the char yield (Faravelli, Frassoldati, Migliavacca, & Ranzi, 2010).

Correlations between yield of several decomposition products and the lignin structure were previously identified, and the char yield was found to be inversely proportional to the amount of hydroxyl and methoxyl groups (Jakab, Faix, & Till, 1997).

The char yields are in the same range as the yields reported by Ma *et al*. (Ma et al., 2015), using the same temperature program. Cellulose displayed a much steeper TGA curve than lignin, a typical behaviour of linear polymers (Figure 5a). This shows clearly in the mass-change rate during the temperature increase, depicted as the first derivative of mass-% (DTG) in Figure 5b. The peak is much sharper for cellulose (E100) than for cellulose-lignin composite fibres (E50-BL50) and lignin. Also, the DTG peak shifts to a higher temperature with increasing lignin concentration.

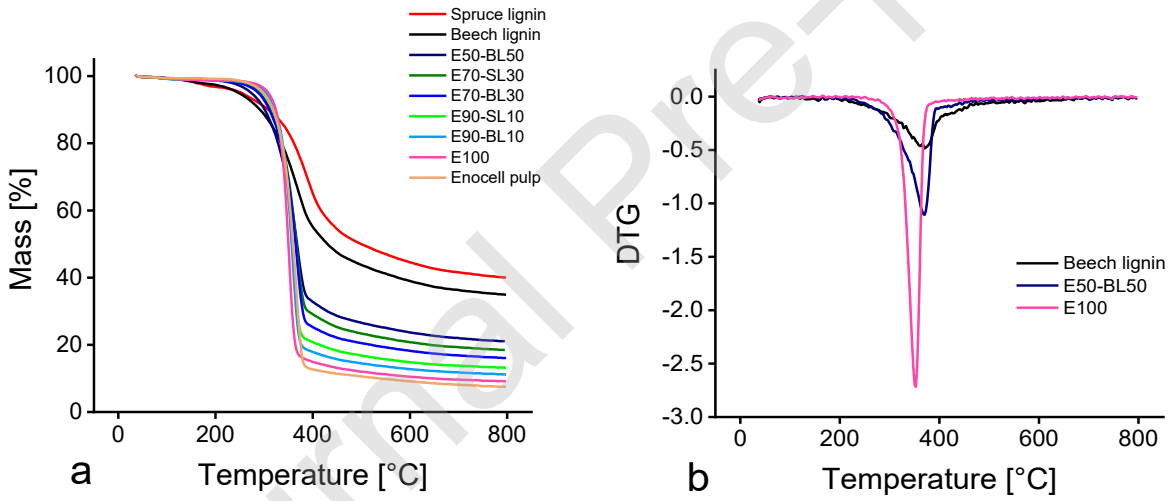

Figure 5. TGA results for PFs and raw materials. Figure (a) shows TGA curves and (b) DTG curves for selected samples.

Pure lignin slowly decomposes over an extended temperature range, giving a lower onset and higher offset temperature than cellulose. This behaviour also transfers to the composite fibres as visualised in Figure 6. Enocell pulp gives an onset temperature of approximately 297°C, an offset temperature of 421°C and a maximum mass loss at 365°C. The lignins exhibit onset temperatures

Journal Pre-proof

of 219°C (BL) / 190°C (SL), offset temperatures of 624°C (BL) / 641°C (SL) and maximum mass loss at 370°C (BL) / 389°C (SL). Yu *et al*. reported similar behaviour of an alkali lignin, with onset temperature at ~200°C and maximum mass loss between 350°C and 400°C (Yu, Paterson, Blamey, & Millan, 2017). The decomposition reaction onset temperature of the composite fibres decreases with their lignin content. This thermal behaviour change with the lignin content in the fibre could be used to adjust the fibre oxidation/stabilization step conditions. This would be advantageous in a continuous carbonisation process, due to potential energy savings.

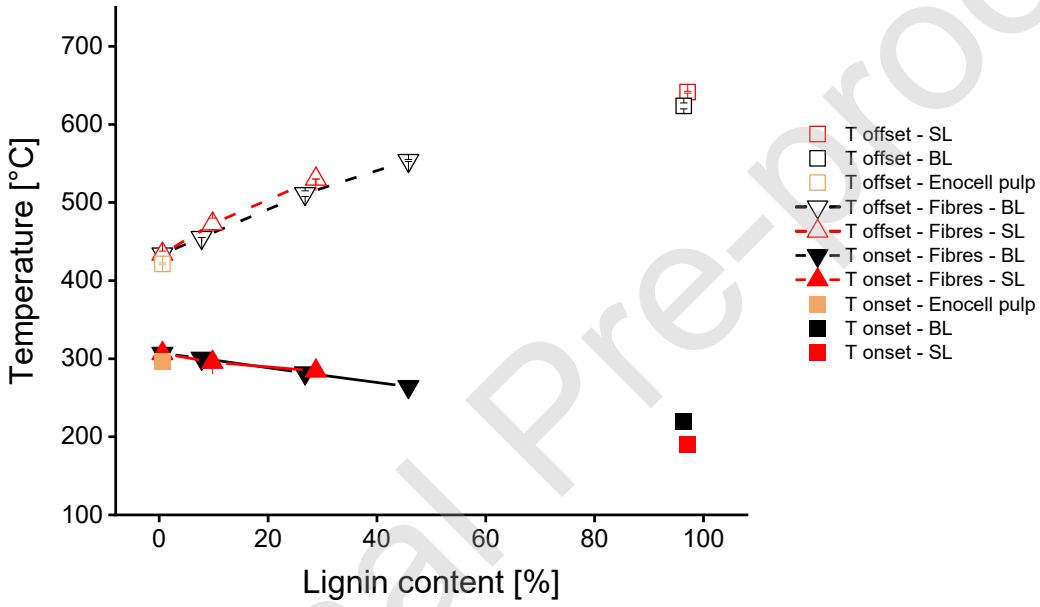

Figure 6. TGA onset and offset temperatures of fibres and raw materials.

To investigate possible synergistic effects in the carbonization of cellulose-lignin composite fibres, the theoretical TGA profile consisting of the weighted sum of cellulose and the respective lignin curves was calculated. The actual composition of the PFs (measured values in Table 3) were used for the calculations. The measured TGA signals show slightly higher char yields than the calculated curves (Figure S8a and S8b in SI, Section 6), but no significant difference in the shape of curves could be observed. However, the measured and calculated DTG curves depicted in Figures S9a-c

Journal Pre-proof

(SI, Section 7), show slight differences. The minimum of the calculated DTG curves are lower, indicating a slightly steeper TGA curve. Also, the minimum of the measured DTG curve appeared at slightly higher temperature than for the calculated curve. The differences in measured and calculated DTG curves indicate some interactions between the components. The slightly higher char yield might also be due to recondensation reactions that are favoured in a matrix where cellulose and lignin are in close contact. Further reduction of the heating rate could promote this effect. Yu *et al*. reported higher char yields for synthetic mixtures containing cellulose and lignin, compared to values estimated based on individual components in the mixture. They also found no significant interactions below 325°C, before the beginning of cellulose carbonization. The maximum weight loss of cellulose and lignin occurs in the same temperature range (350 – 400°C), which contributes to the interactions between the components. Yu *et al*. also reported an increase in char yield from lignin with decreasing heating rate. For cellulose, the influence of heating rate was less evident (Yu et al., 2017).

In all experiments, both oven carbonization test and TG analysis, a heating rate of 10°C/min was used. This heating rate was chosen, as it was suitable for the laboratory devices used, it was not optimised for giving the maximum yield. The yields presented here show the trends for the results with different lignin concentrations in the fibres, but not the maximum yields. By definition, the carbon content of CFs should be ≥ 92% (Frank et al., 2014). The carbon content of CFs produced at 900°C were in the range of 88.6% to 91.7% (Table S6, in SI, Section 8). This can be attributed to the moderate final temperature of 900°C. Higher temperatures were used in the continuation study (part 2), where we focus on the online carbonization of the precursor filaments described herein.

4. Conclusions

Fibres made from cellulose and lignin can be used as precursors for the production of CFs. The purpose of this study was to elucidate the structure of cellulose-lignin composite PFs and their behaviour during carbonization. The PFs were not pre-treated before carbonization to identify

Journal Pre-proof

synergistic effects. Structure and strength of the PFs, are mostly determined by the cellulosic constituent, while the addition of lignin enhances the CF yield. An increase in lignin content decreases the total orientation and tensile strength of the fibre. The decrease of the crystallinity index and the orientation of the cellulose polymers themselves was moderate up to a lignin concentration of 30%. At higher lignin concentration, a clear decrease in the values was observed, indicating that high concentrations of lignin interfere with the alignment of cellulose crystallites.

SWL has been challenging for melt spinning due to a typically high glass transition temperature. This problem is bypassed with solution spinning when SWL is blended with pulp cellulose. Overall, both SL and BL blended with cellulose performed well in the spinning process and gave promising PFs for subsequent carbonization, which is the focus of part 2 of this study.

Acknowledgements

This project has received funding from the European Research Council (ERC) under the European Union's Horizon 2020 research and innovation programme (Grant Agreement No 715788). The authors thank the European Synchrotron Radiation Facility (ESRF) for the provision of beam time at the D2AM beamline.

Journal Pre-proof

Journal Pre-proof

References

Asaadi, S., Hummel, M., Ahvenainen, P., Gubitosi, M., Olsson, U., & Sixta, H. (2018). Structural analysis of Ioncell-F fibres from birch wood. *Carbohydrate Polymers, 181*, 893-901. Retrieved from http://www.sciencedirect.com/science/article/pii/S0144861717313498. doi:https://doi.org/10.1016/j.carbpol.2017.11.062

Ashiotis, G., Deschildre, A., Nawaz, Z., Wright, J. P., Karkoulis, D., Picca, F. E., & Kieffer, J. (2015). The fast azimuthal integration Python library: pyFAI. *Journal of Applied Crystallography, 48*(2), 510-519. Retrieved from https://doi.org/10.1107/S1600576715004306. doi:doi:10.1107/S1600576715004306

Baillères, H., Castan, M., Monties, B., Pollet, B., & Lapierre, C. (1997). Lignin structure in Buxus sempervirens reaction wood. *Phytochemistry, 44*(1), 35-39. Retrieved from http://www.sciencedirect.com/science/article/pii/S0031942296004992. doi:https://doi.org/10.1016/S0031-9422(96)00499-2

Baker, D. A., & Rials, T. G. (2013). Recent advances in low-cost carbon fiber manufacture from lignin. *Journal of Applied Polymer Science, 130*(2), 713-728. Retrieved from https://onlinelibrary.wiley.com/doi/abs/10.1002/app.39273. doi:10.1002/app.39273

Balakshin, M., Berlin, A., Dellicolli, H. T., Grunert, C. A. N. J., Gutman-Maximenko, V., Ortiz, D., & Pye, E. K. (2010a). Derivatives of native lignin as extracted from biomass. *From PCT Int. Appl., WO 2010135804 A1 20101202.*

Balakshin, M., Berlin, A., Dellicolli, H. T., Grunert, C. A. N. J., Gutman-Maximenko, V., Ortiz, D., & Pye, E. K. (2010b). Derivatives of native lignin from hardwood feedstocks. *From PCT Int. Appl., WO 2010135807 A1 20101202.*

Balakshin, M., Berlin, A., Dellicolli, H. T., Grunert, C. A. N. J., Gutman-Maximenko, V., Ortiz, D., & Pye, E. K. (2010c). Derivatives of native lignin from softwood feedstocks. *PCT Int. Appl., WO 2010135806 A1 20101202.*

Balakshin, M., & Capanema, E. (2015). Comprehensive structural analysis of biorefinery lignins with a quantitative 13C NMR approach. *RSC Advances, 5*(106), 87187-87199. Retrieved from http://dx.doi.org/10.1039/C5RA16649G. doi:10.1039/C5RA16649G

Balakshin, M., Capanema, E., & Chang, H.-M. (2008). Recent Advances in Isolation and Analysis of Lignins and Lignin-Carbohydrate Complexes. . In T. Q. Hu (Ed.), *Characterization of Lignocellulosic Materials* (pp. 148–170). Oxford, U.K.: Blackwell Publishing Ltd.

Balakshin, M., Capanema, E., Zhu, X., Sulaeva, I., Potthast, A., Rosenau, T., & Rojas, O. J. (2020). Spruce milled wood lignin: linear, branched or cross-linked? *Green Chemistry*. Retrieved from http://dx.doi.org/10.1039/D0GC00926A. doi:10.1039/D0GC00926A

Beaucage, G. (1995). Approximations Leading to a Unified Exponential/Power-Law Approach to Small-Angle Scattering. *Journal of Applied Crystallography, 28*(6), 717-728. Retrieved from https://onlinelibrary.wiley.com/doi/abs/10.1107/S0021889895005292. doi:10.1107/s0021889895005292

Bengtsson, A., Bengtsson, J., Olsson, C., Sedin, M., Jedvert, K., Theliander, H., & Sjöholm, E. (2018). Improved yield of carbon fibres from cellulose and kraft lignin. *Holzforschung, 72*(12), 1007-1016. Retrieved from https://www.degruyter.com/view/j/hfsg.2018.72.issue-12/hf-2018-0028/hf-2018-0028.xml. doi:10.1515/hf-2018-0028

Bengtsson, A., Bengtsson, J., Sedin, M., & Sjöholm, E. (2019). Carbon Fibers from Lignin-Cellulose Precursors: Effect of Stabilization Conditions. *ACS Sustainable Chemistry & Engineering, 7*(9), 8440-8448. Retrieved from https://doi.org/10.1021/acssuschemeng.9b00108. doi:10.1021/acssuschemeng.9b00108

Bengtsson, A., Hecht, P., Sommertune, J., Ek, M., Sedin, M., & Sjöholm, E. (2020). Carbon Fibers from Lignin–Cellulose Precursors: Effect of Carbonization Conditions. *ACS Sustainable Chemistry & Engineering,*

Journal Pre-proof

8(17), 6826-6833. Retrieved from https://doi.org/10.1021/acssuschemeng.0c01734. doi:10.1021/acssuschemeng.0c01734

Berlin, A., & Balakshin, M. (2014). Chapter 18 - Industrial Lignins: Analysis, Properties, and Applications. In V. K. Gupta, M. G. Tuohy, C. P. Kubicek, J. Saddler, & F. Xu (Eds.), *Bioenergy Research: Advances and Applications* (pp. 315-336). Amsterdam: Elsevier.

Berlin, A., Balakshin, M., Gilkes, N., Kadla, J., Maximenko, V., Kubo, S., & Saddler, J. (2006). Inhibition of cellulase, xylanase and β-glucosidase activities by softwood lignin preparations. *Journal of Biotechnology, 125*(2), 198-209. Retrieved from http://www.sciencedirect.com/science/article/pii/S0168165606001714. doi:https://doi.org/10.1016/j.jbiotec.2006.02.021

Brodin, I., Sjöholm, E., & Gellerstedt, G. (2009). Kraft lignin as feedstock for chemical products: The effects of membrane filtration. *Holzforschung, 63*(3), 290. Retrieved from https://www.degruyter.com/view/j/hfsg.2009.63.issue-3/hf.2009.049/hf.2009.049.xml. doi:10.1515/HF.2009.049

Byrne, N., De Silva, R., Ma, Y., Sixta, H., & Hummel, M. (2018). Enhanced stabilization of cellulose-lignin hybrid filaments for carbon fiber production. *Cellulose, 25*(1), 723-733. Retrieved from https://doi.org/10.1007/s10570-017-1579-0. doi:10.1007/s10570-017-1579-0

Byrne, N., Setty, M., Blight, S., Tadros, R., Ma, Y., Sixta, H., & Hummel, M. (2016). Cellulose-Derived Carbon Fibers Produced via a Continuous Carbonization Process: Investigating Precursor Choice and Carbonization Conditions. *Macromolecular Chemistry and Physics, 217*(22), 2517-2524. Retrieved from https://onlinelibrary.wiley.com/doi/abs/10.1002/macp.201600236. doi:10.1002/macp.201600236

Doucet, M., Cho, J. H., Alina, G., Bakker, J., Bouwman, W., Butler, P., . . . Washington, A. (2017). SasView. Version 4.1.

Edie, D. D. (1998). The effect of processing on the structure and properties of carbon fibers. *Carbon, 36*(4), 345-362. Retrieved from http://www.sciencedirect.com/science/article/pii/S0008622397001851. doi:https://doi.org/10.1016/S0008-6223(97)00185-1

Edison, T. A. (1880). US Patent 223,898.

Ehrnrooth, E. M. L. (1984). Change in Pulp Fibre Density With Acid-Chlorite Delignification. *Journal of Wood Chemistry and Technology, 4*(1), 91-109. Retrieved from https://doi.org/10.1080/02773818408062285. doi:10.1080/02773818408062285

Fagerstedt, K. V., Saranpää, P., Tapanila, T., Immanen, J., Serra, J. A. A., & Nieminen, K. (2015). Determining the Composition of Lignins in Different Tissues of Silver Birch. *Plants (Basel, Switzerland), 4*(2), 183-195. Retrieved from https://pubmed.ncbi.nlm.nih.gov/27135322

https://www.ncbi.nlm.nih.gov/pmc/articles/PMC4844324/. doi:10.3390/plants4020183

Faravelli, T., Frassoldati, A., Migliavacca, G., & Ranzi, E. (2010). Detailed kinetic modeling of the thermal degradation of lignins. *Biomass and Bioenergy, 34*(3), 290-301. Retrieved from http://www.sciencedirect.com/science/article/pii/S0961953409002219. doi:https://doi.org/10.1016/j.biombioe.2009.10.018

Foston, M., Nunnery, G. A., Meng, X., Sun, Q., Baker, F. S., & Ragauskas, A. (2013). NMR a critical tool to study the production of carbon fiber from lignin. *Carbon, 52*, 65-73. Retrieved from http://www.sciencedirect.com/science/article/pii/S0008622312007439. doi:https://doi.org/10.1016/j.carbon.2012.09.006

Frank, E., Steudle, L. M., Ingildeev, D., Spörl, J. M., & Buchmeiser, M. R. (2014). Carbon Fibers: Precursor Systems, Processing, Structure, and Properties. *Angewandte Chemie International Edition, 53*(21), 5262-5298. Retrieved from https://onlinelibrary.wiley.com/doi/abs/10.1002/anie.201306129. doi:10.1002/anie.201306129

Goldhalm, G. (2012). Tencel® Carbon Precursor. *Lenzinger Berichte, 90*, 58-63.

Haslinger, S., Hummel, M., Anghelescu-Hakala, A., Määttänen, M., & Sixta, H. (2019). Upcycling of cotton polyester blended textile waste to new man-made cellulose fibers. *Waste Management, 97*, 88-96. Retrieved from http://www.sciencedirect.com/science/article/pii/S0956053X19305100. doi:https://doi.org/10.1016/j.wasman.2019.07.040

Journal Pre-proof

Ház, A., Jablonský, M., Šurina, I., Kačík, F., Bubeníková, T., & Ďurkovič, J. (2019). Chemical Composition and Thermal Behavior of Kraft Lignins. *Forests, 10*(6), 483. Retrieved from https://www.mdpi.com/1999-4907/10/6/483.

Hosseinaei, O., Harper, D. P., Bozell, J. J., & Rials, T. G. (2016). Role of Physicochemical Structure of Organosolv Hardwood and Herbaceous Lignins on Carbon Fiber Performance. *ACS Sustainable Chemistry & Engineering, 4*(10), 5785-5798. Retrieved from https://doi.org/10.1021/acssuschemeng.6b01828. doi:10.1021/acssuschemeng.6b01828

Hummel, M., Michud, A., Ma, Y., Roselli, A., Stepan, A., Hellstén, S., . . . Sixta, H. (2018). High-performance Lignocellulosic Fibers Spun from Ionic Liquid Solution. In *Cellulose Science and Technology* (pp. 341-370).

Hummel, M., Michud, A., Tanttu, M., Asaadi, S., Ma, Y., Hauru, L. K. J., . . . Sixta, H. (2016). Ionic Liquids for the Production of Man-Made Cellulosic Fibers: Opportunities and Challenges. *Cellulose Chemistry and Properties: Fibers, Nanocelluloses and Advanced Materials*, 133-168. Retrieved from https://doi.org/10.1007/12_2015_307. doi:10.1007/12_2015_307

Imel, A. E., Naskar, A. K., & Dadmun, M. D. (2016). Understanding the Impact of Poly(ethylene oxide) on the Assembly of Lignin in Solution toward Improved Carbon Fiber Production. *ACS Applied Materials & Interfaces, 8*(5), 3200-3207. Retrieved from https://doi.org/10.1021/acsami.5b10720. doi:10.1021/acsami.5b10720

Jakab, E., Faix, O., & Till, F. (1997). Thermal decomposition of milled wood lignins studied by thermogravimetry/mass spectrometry. *Journal of Analytical and Applied Pyrolysis, 40-41*, 171-186. Retrieved from http://www.sciencedirect.com/science/article/pii/S0165237097000466. doi:https://doi.org/10.1016/S0165-2370(97)00046-6

Janson, J. (1970). Calculation of the polysaccharide composition of wood and pulp. *Paperi ja Puu, 52*(5), 323-329.

Kadla, J. F., Kubo, S., Venditti, R. A., Gilbert, R. D., Compere, A. L., & Griffith, W. (2002). Lignin-based carbon fibers for composite fiber applications. *Carbon, 40*(15), 2913-2920. Retrieved from http://www.sciencedirect.com/science/article/pii/S0008622302002488. doi:https://doi.org/10.1016/S0008-6223(02)00248-8

Koch, G. (2006). Raw Material for Pulp. In *Handbook of Pulp* (pp. 21-68).

Kubo, S., & Kadla, J. (2005a). Kraft lignin/poly(ethylene oxide) blends: Effect of lignin structure on miscibility and hydrogen bonding. *Journal of Applied Polymer Science, 98*(3), 1437-1444. Retrieved from https://onlinelibrary.wiley.com/doi/abs/10.1002/app.22245. doi:10.1002/app.22245

Kubo, S., & Kadla, J. (2005b). Lignin-based Carbon Fibers: Effect of Synthetic Polymer Blending on Fiber Properties. *Journal of Polymers and the Environment, 13*(2), 97-105. Retrieved from https://doi.org/10.1007/s10924-005-2941-0. doi:10.1007/s10924-005-2941-0

Langan, P., Petridis, L., O'Neill, H. M., Pingali, S. V., Foston, M., Nishiyama, Y., . . . Davison, B. H. (2014). Common processes drive the thermochemical pretreatment of lignocellulosic biomass. *Green Chemistry, 16*(1), 63-68. Retrieved from http://dx.doi.org/10.1039/C3GC41962B. doi:10.1039/C3GC41962B

Lenz, J., Schurz, J., & Wrentschur, E. (1994). On the Elongation Mechanism of Regenerated Cellulose Fibres. *Holzforschung, 48*(s1), 72. Retrieved from https://www.degruyter.com/view/j/hfsg.1994.48.issue-s1/hfsg.1994.48.s1.72/hfsg.1994.48.s1.72.xml. doi:10.1515/hfsg.1994.48.s1.72

Ma, Y., Asaadi, S., Johansson, L.-S., Ahvenainen, P., Reza, M., Alekhina, M., . . . Sixta, H. (2015). High-Strength Composite Fibers from Cellulose–Lignin Blends Regenerated from Ionic Liquid Solution. *ChemSusChem, 8*(23), 4030-4039. Retrieved from https://onlinelibrary.wiley.com/doi/abs/10.1002/cssc.201501094. doi:10.1002/cssc.201501094

Ma, Y., Hummel, M., Määttänen, M., Särkilahti, A., Harlin, A., & Sixta, H. (2016). Upcycling of waste paper and cardboard to textiles. *Green Chemistry, 18*(3), 858-866. Retrieved from http://dx.doi.org/10.1039/C5GC01679G. doi:10.1039/C5GC01679G

Mainka, H., Täger, O., Körner, E., Hilfert, L., Busse, S., Edelmann, F. T., & Herrmann, A. S. (2015). Lignin – an alternative precursor for sustainable and cost-effective automotive carbon fiber. *Journal of Materials Research and Technology, 4*(3), 283-296. Retrieved from

Journal Pre-proof

http://www.sciencedirect.com/science/article/pii/S2238785415000599. doi:https://doi.org/10.1016/j.jmrt.2015.03.004

Morgan, P. (2005). *Carbon Fibers and Their Composites* (1st ed.). Boca Raton: CRC Press.

Norberg, I., Nordström, Y., Drougge, R., Gellerstedt, G., & Sjöholm, E. (2013). A new method for stabilizing softwood kraft lignin fibers for carbon fiber production. *Journal of Applied Polymer Science, 128*(6), 3824-3830. Retrieved from https://onlinelibrary.wiley.com/doi/abs/10.1002/app.38588. doi:10.1002/app.38588

Nordström, Y., Norberg, I., Sjöholm, E., & Drougge, R. (2013). A new softening agent for melt spinning of softwood kraft lignin. *Journal of Applied Polymer Science, 129*, 1274-1279. doi:10.1002/app.38795

Nypelö, T., Asaadi, S., Kneidinger, G., Sixta, H., & Konnerth, J. (2018). Conversion of wood-biopolymers into macrofibers with tunable surface energy via dry-jet wet-spinning. *Cellulose, 25*(9), 5297-5307. Retrieved from https://www.scopus.com/inward/record.uri?eid=2-s2.0-85048809738&doi=10.1007%2fs10570-018-1902-4&partnerID=40&md5=ef57e98501451e9a491290510e90d23d. doi:10.1007/s10570-018-1902-4

Potthast, A., Radosta, S., Saake, B., Lebioda, S., Heinze, T., Henniges, U., . . . Wetzel, H. (2015). Comparison testing of methods for gel permeation chromatography of cellulose: coming closer to a standard protocol. *Cellulose, 22*(3), 1591-1613. Retrieved from https://doi.org/10.1007/s10570-015-0586-2. doi:10.1007/s10570-015-0586-2

Prosen, S. P. (1970). Carbon resin composites. *Fibre Science and Technology, 3*(2), 81-104. Retrieved from http://www.sciencedirect.com/science/article/pii/0015056870900163. doi:https://doi.org/10.1016/0015-0568(70)90016-3

Röder, T., Moosbauer, J., Kliba, G., Schlader, S., Zuckerstätter, G., & Sixta, H. (2009). Comparative characterization of man-made regenerated cellulose fibres. *Lenzinger Berichte, 87*, 98-105.

Röder, T., Moosbauer, J., Wöss, K., Schlader, S., & Kraft, G. (2013). Man-made cellulose fibers–a comparison based on morphology and mechanical properties. *Lenzinger Berichte, 91*, 7-12.

Sayyed, A., Deshmukh, N., & Pinjari, D. (2019). A critical review of manufacturing processes used in regenerated cellulosic fibres: viscose, cellulose acetate, cuprammonium, LiCl/DMAc, ionic liquids, and NMMO based lyocell. *Cellulose, 26*, 2913-2940. doi:10.1007/s10570-019-02318-y

Sharma, A., Sen, D., Thakre, S., & Kumaraswamy, G. (2019). Characterizing Microvoids in Regenerated Cellulose Fibers Obtained from Viscose and Lyocell Processes. *Macromolecules, 52*(11), 3987-3994. Retrieved from https://doi.org/10.1021/acs.macromol.9b00487. doi:10.1021/acs.macromol.9b00487

Sixta, H., Michud, A., Hauru, L., Asaadi, S., Ma, Y., King Alistair, W. T., . . . Hummel, M. (2015). Ioncell-F: A High-strength regenerated cellulose fibre. *Nordic Pulp & Paper Research Journal, 30*(1), 43-57. Retrieved from https://www.degruyter.com/view/j/npprj.2015.30.issue-1/npprj-2015-30-01-p043-057/npprj-2015-30-01-p043-057.xml. doi:10.3183/npprj-2015-30-01-p043-057

Stamm, A. J. (1929). Density of Wood Substance, Adsorption by Wood, and Permeability of Wood. *The Journal of Physical Chemistry, 33*(3), 398-414. Retrieved from https://doi.org/10.1021/j150297a008. doi:10.1021/j150297a008

Swan, J. W. (1880). US Patent 233,445.

Unterweger, C., Hinterreiter, A., Stifter, D., & Fuerst, C. (2018). *Cellulose-Based Carbon Fibers: Increasing Tensile Strength and Carbon Yield*. Paper presented at the Carbon 2018, Madrid, Spain.

Wang, L., Ago, M., Borghei, M., Ishaq, A., Papageorgiou, A. C., Lundahl, M., & Rojas, O. J. (2019). Conductive Carbon Microfibers Derived from Wet-Spun Lignin/Nanocellulose Hydrogels. *ACS Sustainable Chemistry and Engineering, 7*(6), 6013-6022. Retrieved from https://www.scopus.com/inward/record.uri?eid=2-s2.0-85063064526&doi=10.1021%2facssuschemeng.8b06081&partnerID=40&md5=8f73b4b966328dbebcded2bb85e72839. doi:10.1021/acssuschemeng.8b06081

Vickers, M. E., Briggs, N. P., Ibbett, R. N., Payne, J. J., & Smith, S. B. (2001). Small angle X-ray scattering studies on lyocell cellulosic fibres: the effects of drying, re-wetting and changing coagulation temperature. *Polymer, 42*(19), 8241-8248. Retrieved from http://www.sciencedirect.com/science/article/pii/S003238610100266X. doi:https://doi.org/10.1016/S0032-3861(01)00266-X

Journal Pre-proof

Yang, M., Zhao, W., Singh, S., Simmons, B., & Cheng, G. (2019). On the solution structure of kraft lignin in ethylene glycol and its implication for nanoparticle preparation. *Nanoscale Advances, 1*(1), 299-304. Retrieved from http://dx.doi.org/10.1039/C8NA00042E. doi:10.1039/C8NA00042E

Yu, J., Paterson, N., Blamey, J., & Millan, M. (2017). Cellulose, xylan and lignin interactions during pyrolysis of lignocellulosic biomass. *Fuel, 191*, 140-149. Retrieved from http://www.sciencedirect.com/science/article/pii/S0016236116311589. doi:https://doi.org/10.1016/j.fuel.2016.11.057

Zhang, B., Lu, C., Liu, Y., Zhou, P., Yu, Z., & Yuan, S. (2019). Wet spun polyacrylonitrile-based hollow-mesoporous fibers with different draw ratios. *Polymer, 179*, 121618. Retrieved from https://www.scopus.com/inward/record.uri?eid=2-s2.0-85068233126&doi=10.1016%2fj.polymer.2019.121618&partnerID=40&md5=b15e0ef0d041afdc99891a001ab16c4e. doi:10.1016/j.polymer.2019.121618

Zhang, M., & Ogale, A. A. (2014). Carbon fibers from dry-spinning of acetylated softwood kraft lignin. *Carbon, 69*, 626-629. Retrieved from http://www.sciencedirect.com/science/article/pii/S0008622313011573. doi:https://doi.org/10.1016/j.carbon.2013.12.015

Journal Pre-proof

Journal Pre-proof

Table 1. Summary and sample codes of produced PFs

Enocell pulp in dope [%]	Lignin in dope [%]	Lignin Type	Dope Total Conc. [%]	Fibre code	DR*
100	0	-	13	E100	3, 6, 9 and 12
90	10	Beech	13	E90-BL10	3, 6, 9 and 12
70	30	Beech	15	E70-BL30	3, 6, 9 and 12
50	50	Beech	17	E50-BL50	3, 6, 9 and 12
90	10	Spruce	13	E90-SL10	3, 6, 9 and 12
70	30	Spruce	15	E70-SL30	3, 6, 9 and 12

*Draw ratio, $\mathrm{DR} = \frac{\text{Take-up velocity}}{\text{Extrusion velocity}}$

Table 2. Properties of cellulose and lignin raw materialsThe analysis of the lignin structure with

Raw Material	Code	M_w [kg/mol]	M_n [kg/mol]	Cellulose [%]	Hemicell. [%]	Lignin [%]	Carbo-hydrates [%]	Ash *) [%]	Other [%]
Enocell pulp	E	163.6	57.5	91.7	7.7	0.6			
Beech lignin	BL	2.23	0.440			96.4	0.3	0.2	3.1
Spruce lignin	SL	5.89	0.535			97.1	0.5	0.2	2.2

*) Determined according to T 211 om-02

Journal Pre-proof

Table 3. Carbohydrate and lignin content of precursor fibres (DR 6) – Measured and theoretical values.

	Measured			Theoretical		
Sample	Cellulose [%]	Hemicell. [%]	Lignin [%]	Lignin [%]	Relative lignin loss [%]	Titer [dtex]
E100	91.9	7.5	0.6	0.6	0.0	2.30
E90-BL10	85.6	6.6	7.8	10.2	23.5	2.24
E70-BL30	67.7	5.5	26.8	29.3	8.5	2.67
E50-BL50	50.2	4.0	45.8	48.5	5.6	3.10
E90-SL10	84.1	6.1	9.8	10.3	4.9	2,34
E70-SL30	65.3	5.9	28.8	29.6	2.7	2.73

Table 4. Crystalline parameters of PFs (DR3) with different lignin content.

Sample Fibre code	CEL.I	C.I.EQ.	f_{WAXD}	Ave. CW [Å]
E100	89	59	0.88	38
E90-BL10	83	55	0.86	38
E70-BL30	66	53	0.84	36
E50-BL50	45	38	0.76	36
E90-SL10	79	60	0.87	38
E70-SL30	64	56	0.85	37

CEL.I: index for the cellulose content in the fibre
C.I.EQ.: Crystallinity index from equatorial scattering of fibre diffraction
f_{WAXD}: Hermans orientation parameter
Ave. CW: average width of three crystal lattice planes

Journal Pre-proof